Mon. Not. R. Astron. Soc. **000**, 1–11 (2010) Printed 21 April 2010 (MN LATEX style file v2.2)

Mass models from high-resolution HI data of the dwarf galaxy NGC 1560

G. Gentile[1], M. Baes[1], B. Famaey[2], K. Van Acoleyen[1]
[1]*Department of Physics and Astronomy, Universiteit Gent, Krijgslaan 281, B-9000 Gent, Belgium*
[2]*Observatoire Astronomique, Université de Strasbourg, CNRS UMR 7550, F-67000 Strasbourg, France*

Accepted ... Received ... ; in original form ...

ABSTRACT

We present HI observations performed at the GMRT of the nearby dwarf galaxy NGC 1560. This Sd galaxy is well-known for a distinct "wiggle" in its rotation curve. Our new observations have twice the resolution of the previously published HI data. We derived the rotation curve by taking projection effects into account, and we verified the derived kinematics by creating model datacubes. This new rotation curve is similar to the previously published one: we confirm the presence of a clear wiggle. The main differences are in the innermost $\sim 100''$ of the rotation curve, where we find slightly ($\lesssim 5$ km s^{-1}) higher velocities. Mass modelling of the rotation curve results in good fits using the core-dominated Burkert halo (which however does not reproduce the wiggle), bad fits using the a Navarro, Frenk & White halo, and good fits using MOND (Modified Newtonian Dynamics), which also reproduces the wiggle.

Key words: galaxies: kinematics and dynamics - dark matter - galaxies: spiral - gravitation - galaxies: individual: NGC 1560

1 INTRODUCTION

Rotation curves of spiral galaxies are one of the most important tools to investigate the content and distribution of dark matter in galaxies. They have been used for a variety of purposes, in particular to investigate their systematic properties (Persic, Salucci & Stel 1996, Salucci et al. 2007, Gentile 2008), to test the validity of the predictions of the Cold Dark Matter (CDM) theory (e.g., de Blok et al. 2001, Marchesini et al. 2002, Gentile et al. 2004, 2005, 2007a, Kuzio de Naray et al. 2006, Corbelli et al. 2010), or to study the connection between the distributions of dark and luminous matter (Broeils 1992, McGaugh et al. 2000, McGaugh 2005a, Gentile et al. 2009, Donato et al. 2009).

Testing the validity of the CDM predictions is a very important issue, because (CDM-only) simulations result in dark matter halos with an almost universal density profile (the details of how universal the profile actually is have extensively been discussed in the literature), which is well described by the NFW (Navarro, Frenk & White 1996) halo, characterised by a central density cusp (the density ρ is proportional to r^{-1} when the radius r tends to zero, but see also Section 6), whereas observations tend to indicate the presence of a constant density core. The influence of baryons on the distribution of dark matter is a crucial point; however, there is no general consensus about what the dominant effect(s) is(are). A non-exhaustive list of ways by which baryons can change the distribution of dark matter includes: adiabatic contraction (Blumenthal et al. 1986, Gnedin et al. 2004, Sellwood & McGaugh 2005), the influence of bars (e.g., Weinberg & Katz 2002, McMillan & Dehnen 2005, Sellwood 2008), or the influence of gas (Mashchenko, Couchman & Wadsley 2006, Governato et al. 2010). Because of the additional complication brought by baryons, dwarf galaxies and low surface brightness (LSB) galaxies are better suited for deriving the properties of dark matter in galaxies.

An alternative explanation to dark matter in galaxies is MOND (Modified Newtonian Dynamics, introduced by Milgrom 1983), where the effective gravitational acceleration becomes stronger than expected in the Newtonian case, when the gravitational acceleration falls below a critical value, $a_0 \sim 1.2 \times 10^{-8}$ cm s^{-2}. MOND explains very well the observed kinematical properties of galaxies: LSB galaxies (McGaugh & de Blok 1998), tidal dwarf galaxies (Gentile et al. 2007b), the Milky Way (Famaey, Bruneton & Zhao 2007a, McGaugh 2008, Bienaymé et al. 2009), early-type spiral galaxies (Sanders & Noordermeer 2007), elliptical galaxies (Milgrom & Sanders 2003, Tiret et al. 2007), and galaxy scaling relation in general, such as the baryonic Tully-Fisher relation (McGaugh 2005b). However, let us note that the MOND prescription is not sufficient to explain the observed discrepancy between luminous and dynamical mass in galaxy clusters (e.g. Angus et al. 2007).

The dwarf galaxy NGC 1560, whose rotation curve was derived by Broeils (1992, hereafter B92) based on WSRT (Westerbork Synthesis Radio Telescope) observations, is a nearby Sd galaxy with an absolute B-band magnitude of $M_{\rm B} = -16.6$ (Krismer et al. 1995, assuming a distance of 3.5 Mpc). Estimates of its distance

Table 1. Observational parameters of the HI observations with the GMRT.

Observing dates	13-14 Sep 2007
Time on source (mins)	690
Synthesized beam	$8.1'' \times 6.4''$
Number of velocity channels	128
Velocity increment	6.7 km s^{-1}
rms noise in the channel maps	0.8 mJy beam^{-1}

vary significantly from one study to another: values from 2.5 Mpc (Lee & Madore 1993) to 3.7 Mpc (Sandage 1988) can be found. B92 assumed a distance of 3 Mpc. Karachentsev et al. (2003) find 3.45 ± 0.36 Mpc from the tip of the red giant branch method, using HST data. We assume this value unless stated otherwise, because it is one of the most accurate to date.

NGC 1560 is a very interesting galaxy to study because it is the stereotypical galaxy displaying what is known as "Renzo's rule" (from Sancisi 2004): for every feature in the distribution of visible matter there is a corresponding feature in the total distribution of matter. In the rotation curve of NGC 1560, as derived by B92, there is a clear "wiggle" in the total rotation velocity, which corresponds very closely to a similar wiggle in the gas contribution to the rotation curve. Mass models such as MOND naturally reproduce the feature, whereas models that include a dominant spherical (or triaxial) halo are too smooth to do so. This motivated us to re-observe NGC 1560 at higher resolution, to independently trace the rotation curve and probe the region around the velocity wiggle.

In the present paper, we present an analysis of HI observations performed with the GMRT (Giant Metrewave Radio Telescope) which have a spatial resolution almost two times better than the data presented in B92. We re-derive the rotation curve and make mass models, with various assumptions concerning the distribution of dark matter.

2 OBSERVATIONS

The observations were performed on 13-14 September 2007 at the GMRT. The correlator setup was such that the total bandwidth was 2 MHz, with 128 channels centred around a heliocentric (optical definition) systemic velocity of -36 km s^{-1}. After Hanning smoothing, the velocity resolution of our datacube is 6.7 km s^{-1}. Standard calibration and editing procedures were performed within the AIPS (Astronomical Image Processing System) software package. The absolute flux and bandpass calibration were performed using the standard calibrators 3C 48 and 3C 147, whereas the phase calibrator was chosen to be 0410+769. After calibration, the data were continuum-subtracted using line-free channels on either side of the channels with line emission.

Imaging was performed using the task IMAGR in AIPS. To avoid resolving excessively the extended structure, after various attempts we decided that a Gaussian taper of 25 kλ provides a good compromise between resolution and sensitivity to extended emission. The synthesized beam of our final high-resolution maps is $8.1'' \times 6.4''$, which is almost a factor of 2 better than B92 (whose beam size was $14'' \times 13''$). In the first maps we produced, we noticed the presence of a weak "negative bowl" around the emission, characteristic of missing short-spacing information. However, following Greisen, Spekkens & van Moorsel (2009), we used the technique of multi-scale CLEAN, which they found can eliminate most of the negative flux around the emission, and thus solve almost completely the missing short-spacing problem. As we explain in the next section, the use of multi-scale CLEAN likely enabled us to recover most of the HI flux of NGC 1560.

3 HI IN NGC 1560

The final high-resolution datacube is shown in Fig. 1. One can notice that the emission traces the rotation of a highly inclined (but not fully edge-on) disk. The rms noise in the channel maps is 0.8 mJy beam^{-1}. A few channels around zero velocity have significantly higher noise, which can be explained by the presence of very diffuse, low-surface brightness emission due to galactic HI.

The total HI flux (calculated from the primary beam corrected low-resolution cube) is 294.6 Jy km s^{-1}, which is 23 % lower than B92, but is consistent with the single-dish total flux of 290 Jy km s^{-1} given by de Vaucouleurs et al. (1991). Importantly, the total flux of our HI datacube derived with the point-source CLEAN would have been 32 % lower, showing the ability of multi-scale CLEAN to deal with short spacing data. The total HI map (moment-0 map) is given in Fig. 2.

To better study the extended, low surface brightness emission, we constructed a low-resolution datacube with a beam of $25'' \times 25''$. The resulting total HI map, superimposed with an optical image of NGC 1560, is shown in Fig. 3.

We derived the surface density profile by averaging over ellipses using the geometrical parameters derived in the next section. Small changes in the geometrical parameters do not affect significantly the resulting surface density profile, which is shown in Fig. 4. Similarly to what B92 found, the HI distribution is quite symmetric, apart from the "bump" around 300-350 $''$, which is very promiment on the northern side and just hinted at on the southern side.

4 ROTATION CURVE

The velocity field of NGC 1560 was derived using the WAMET method (Gentile et al. 2004, where the velocity in each position of the velocity field is derived using only the side of the velocity profile opposite to the systemic velocity), which gives better results than traditional methods (such as the intensity-weighted mean) when projection and/or resolution effects are expected to be non-negligible. In the case of NGC 1560, because of its high inclination angle, projection effects could potentially bias towards lower rotation velocities (see e.g. Sancisi & Allen 1979), therefore we decided to use the method described in Gentile et al. (2004) instead of the intensity-weighted mean. The velocity field, overlaid with the total HI map, is shown in Fig. 6.

Once the velocity field was constructed, we derived the rotation curve using the task ROTCUR in GIPSY (Groningen Imaging Processing System), which makes a tilted-ring model of the velocity field (Begeman 1989). Several attempts were made to leave as many free parameters as possible, and at the same time have stable solutions for the rings with enough points. We ended up leaving as free parameters (apart from the rotation velocity) the position angle and the systemic velocity. The inclination was fixed at its average value.

Then, based on the rotation curve, the geometrical parameters derived from the tilted-ring modelling of the velocity field, on an assumed scale-height of the HI layer of 0.2 kpc (Barbieri et al., 2005), an HI velocity dispersion of 10 km s^{-1} (Tamburro et al.,

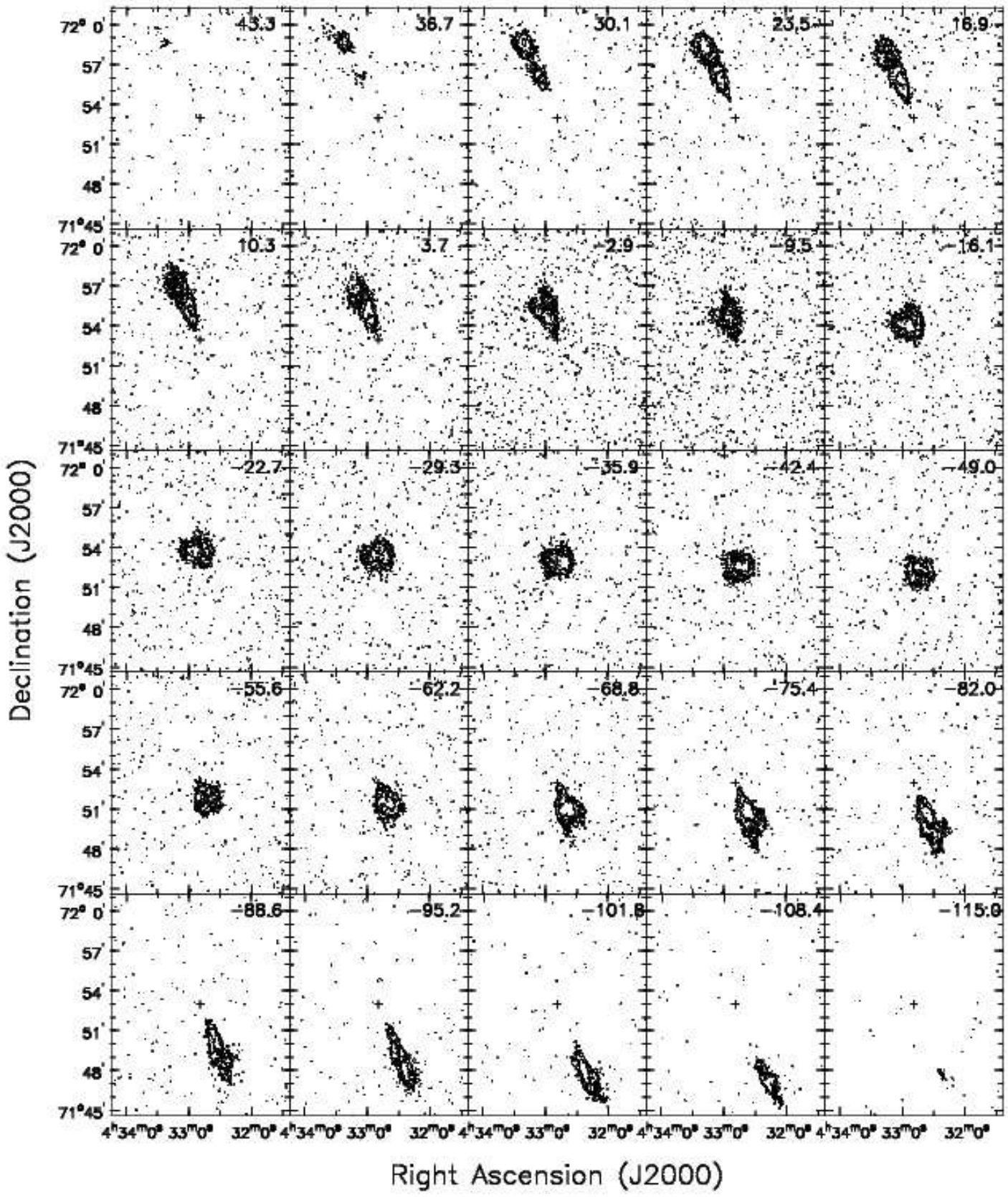

Figure 1. Observed channel maps of NGC 1560. The heliocentric radial velocity (in km s^{-1}) is indicated at the top right corner of each channel map. Contours are -2.5, 2.5 ($\sim 3\sigma$), 5, 10, 20, 40 mJy $beam^{-1}$. The cross shows the location of the galaxy centre. The synthesized beam is $8.1'' \times 6.4''$.

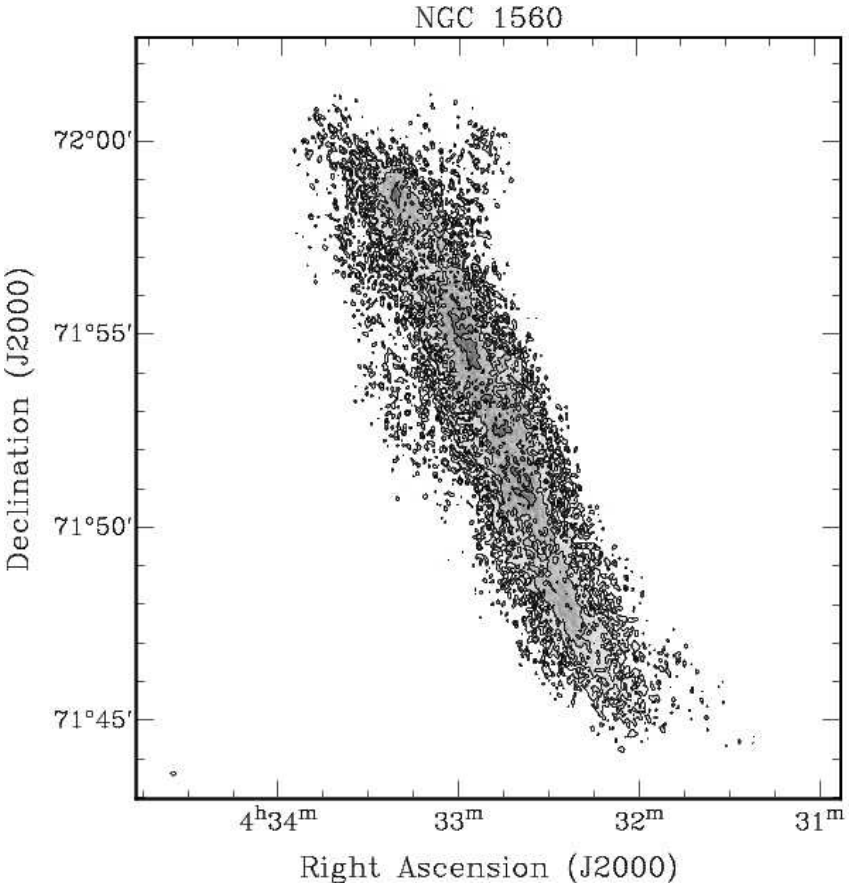

Figure 2. Total HI map based on the high-resolution datacube. Contours are (8, 16, 32, 64)$\times 10^{20}$ atom cm^{-2}. The lowest contour represents the "pseudo-3σ" level defined in the same way as Verheijen & Sancisi (2001). The synthesized beam is $8.1'' \times 6.4''$.

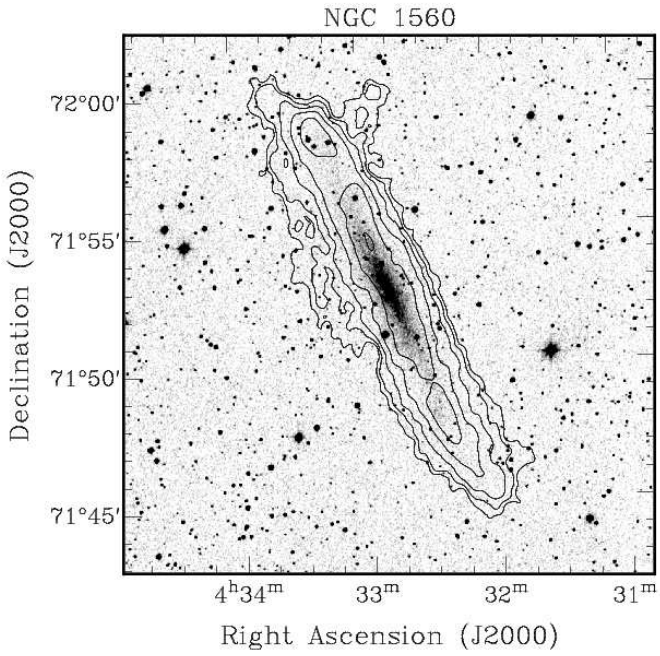

Figure 3. Total HI map based on the low-resolution datacube, overlaid with an optical (DSS) image. Contours are (1, 2, 4, 8, 16, 32, 64)$\times 10^{20}$ atom cm^{-2}). The lowest contour represents the "pseudo-3σ" level defined in the same way as Verheijen & Sancisi (2001). The synthesized beam is $25'' \times 25''$.

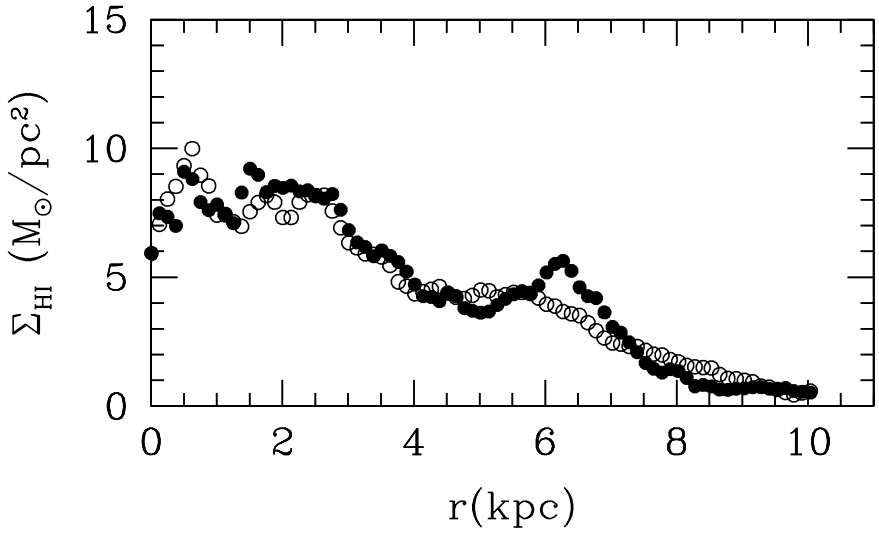

Figure 4. HI surface density, calculated from averaging over ellipses, as a function of radius. Full/empty circles represent the northern/southern half of the galaxy.

2009), and the surface density profile, we built model datacubes to check the validity of our derived parameters. Comparison with the data was made channel map by channel map and on the moment maps. In particular, it turns out that, in order to reproduce the total HI map, the inclination angle had to be changed from 78° to 82° (and the rotation velocity was corrected by a factor sin(78°)/sin(82°)). This is illustrated in Fig. 5. Once this change was made, the agreement between the model datacube and the observed one is excellent, as can be seen in Fig. 7. Also, contrary to Gentile et al. (2007a), the central channel maps are well reproduced without the need of introducing non-circular motions in the model datacube.

The rotation curve (Fig. 8) is very similar to the one derived by B92. The last four points of the rotation curve were derived using the velocity field made from the low-resolution data cube. The largest differences between our rotation curve and the one derived by B92 are of order $\lesssim 5$ km s^{-1} in the innermost $\sim 100''$, where projection effects are expected to be stronger. Then, before making the mass models, the rotation curve was corrected for asymmetric drift following B92 and Skillman et al. (1987). The corrections were smaller than the errorbars. For the last three data points of the rotation curve (when the surface density, of at least one side of the galaxy, drops below 1 M$_\odot$ pc^{-2}), we did not apply the correction, as it would be too uncertain because it would imply dividing by values of the surface density very close to zero. The errorbars on the rotation curve were calculated from the difference between the approaching and the receding side; a minimum realistic error of 2 km s^{-1} was taken into account. The rotation curve determined separately for the two sides of the galaxy is shown in Fig. 9. Similarly to what B92 had found, we find that globally the rotation curve is quite symmetric, but that in the region between 200″ and 350″ the asymmetries are largest, typically of order $6-7$ km s^{-1}. We note that the wiggle is clearly present on one side (the northern side) and barely visible on the other side; in this respect, the kinematic asymmetry is very similar to the surface density asymmetry.

5 MASS MODELS

5.1 The contribution of visible matter

The contribution of the gaseous disk to the rotation curve ($V_{\rm gas}$) was derived using the task ROTMOD in GIPSY, which makes use of the method outlined in Casertano (1983). We used the surface density profile derived in Section 3 and we assumed the same scale-height as in our model datacubes, i.e. 0.2 kpc. Different (but realistic) values of the scale-height do not affect $V_{\rm gas}$ significantly. The HI surface density distribution was then multiplied by a factor 1.33 to account for primordial helium.

In order to derive the shape of the contribution of the stellar disk to the rotation curve ($V_{\rm stars}$), we applied the ROTMOD to the I-band photometric data obtained by Buta & McCall (1999). Also in this case, we assumed a scale-height of 0.2 kpc. Using the range of major-axis scale lengths given in Buta & McCall, and assuming that the scale length/scale height ratio is 7.3 (Kregel, van der Kruit & de Grijs 2002), we find a possible range of scale heights of $0.13-0.37$ kpc. Again, assuming an infinitely thin disk or a thicker - but realistic - disk would not significantly change the resulting $V_{\rm stars}$. The absolute scaling of $V_{\rm stars}$ depends on the stellar mass-to-light (M/L) ratio. One way of estimating its value is from stellar population synthesis models, which find a correlation between observed colour and M/L ratio. We used the method described in Bell & de Jong (2001), and from the $(V-I)$ colour given in Buta & McCall (1999) we found and I-band ($M/L_{\rm I}$) mass-to-light ratio of 1.43. A secure assessment of the uncertainty on this value is virtually impossible to give, because it combines observational and theoretical uncertainties. We estimate it to be around 0.2 dex (de Jong & Bell 2007), therefore in our fits we leave $M/L_{\rm I}$ as a free parameter, constrained within 0.2 dex around 1.43.

5.2 Dark matter and MOND

To explain the mass discrepancy in NGC 1560, one has to resort to either a dark matter halo or MOND.

For the dark matter halo, we considered two different possibilities: a Burkert halo and an NFW halo (see also Section 6 for

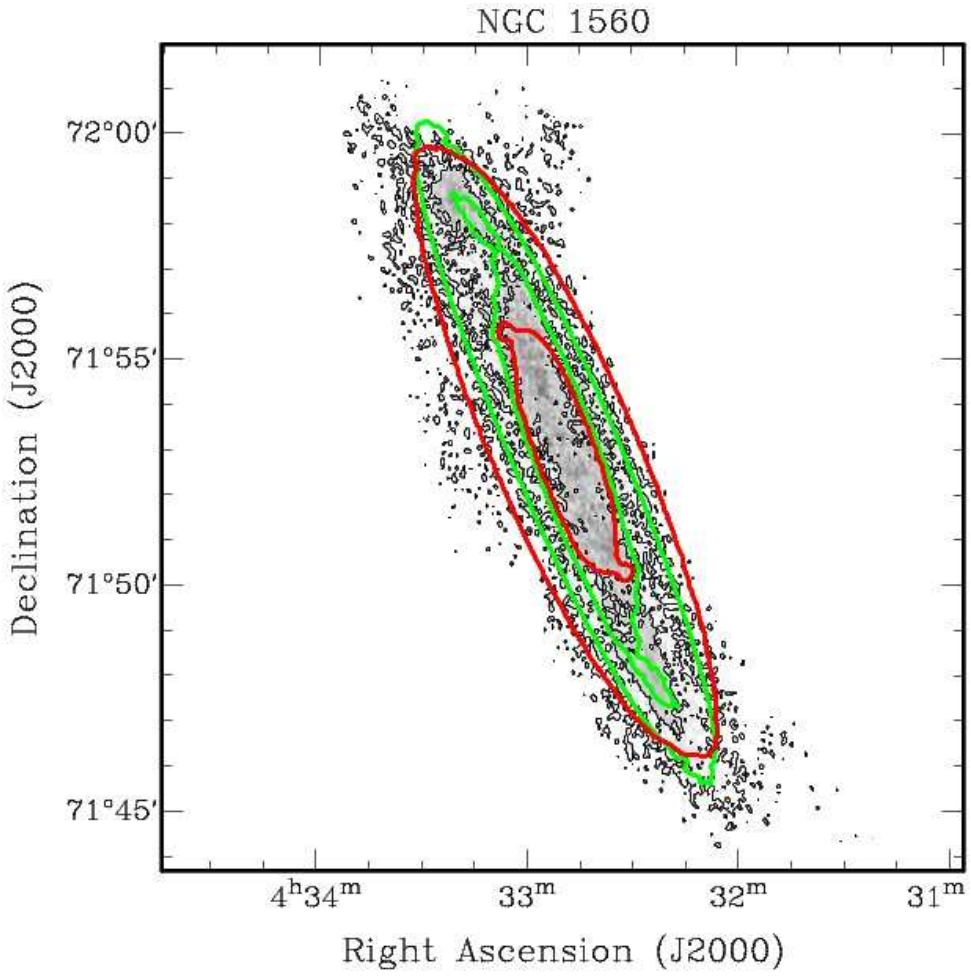

Figure 5. Comparison of the observed total HI map (black contours and greyscale) with the total HI map derived from a model datacube assuming an inclination angle of 78° (red contours) and 82° (green contours). An inclination angle of 82° gives a better representation of the observations. Contours are 1 and 3 $\times 10^{21}$ atom cm^{-2}.

a discussion of the Einasto halo). The Burkert halo (Burkert 1995, Salucci & Burkert 2001) is an empirical functional form for the density distribution of dark matter in galaxies ($\rho_{\rm Bur}$), which generally gives good fits to rotation curves:

$$\rho_{\rm Bur}(r) = \frac{\rho_0 r_{\rm core}^3}{(r + r_{\rm core})(r^2 + r_{\rm core}^2)} \quad (1)$$

were ρ_0 is the central density and $r_{\rm core}$ is the core radius. The Burkert halo has a constant density core at the centre.

The NFW halo (Navarro, Frenk & White 1996) is the result of an analytical fit to the dark matter density distribution that comes out of cosmological simulations performed within the frame of the (Λ)CDM theory. The density distribution $\rho_{\rm NFW}(r)$ is given by

$$\rho_{\rm NFW}(r) = \frac{\rho_{\rm s}}{(r/r_{\rm s})(1 + r/r_{\rm s})^2}, \quad (2)$$

where $\rho_{\rm s}$ and $r_{\rm s}$ are the characteristic density and scale of the NFW halo. A more useful pair of parameters can be found in the concentration parameter ($c_{\rm vir}$) and the virial mass ($M_{\rm vir}$). Cosmological simulations show that these two parameters are in fact correlated (Bullock et al. 2001, Wechsler et al. 2002, Neto et al. 2007), so that the following relations apply:

$$c_{\rm vir} \simeq 13.6 \left(\frac{M_{\rm vir}}{10^{11}{\rm M}_\odot}\right)^{-0.13} \quad (3)$$

$$r_{\rm s} \simeq 8.8 \left(\frac{M_{\rm vir}}{10^{11}{\rm M}_\odot}\right)^{0.46} {\rm kpc} \quad (4)$$

$$\rho_{\rm s} \simeq \frac{\Delta}{3} \frac{c_{\rm vir}^3}{\ln(1 + c_{\rm vir}) - c_{\rm vir}/(1 + c_{\rm vir})} \rho_{\rm crit} \quad (5)$$

where Δ is the virial overdensity at $z = 0$; it can be calculated following Bryan & Norman (1998).

An alternative explanation to the presence of dark matter in galaxies is MOND. In MOND, the true gravitational acceleration $\vec{g}$ can be computed from the Newtonian acceleration $\vec{g_{\rm N}}$ through the following relation:

$$\vec{g} = \vec{g_{\rm N}}/\mu(|g|/a_0) \quad (6)$$

where $a_0 \sim 1.2 \times 10^{-8}$ cm s^{-2} (Begeman, Broeils & Sanders 1991), and $\mu(x)$ is the so-called interpolating function, whose asymptotic values are $\mu(x) = x$ when $x \ll 1$ and $\mu(x) = 1$ when $x \gg 1$. The exact functional form of $\mu(x)$ is not defined by MOND, and we adopt here the "simple" interpolating function (Famaey & Binney 2005, Zhao & Famaey 2006):

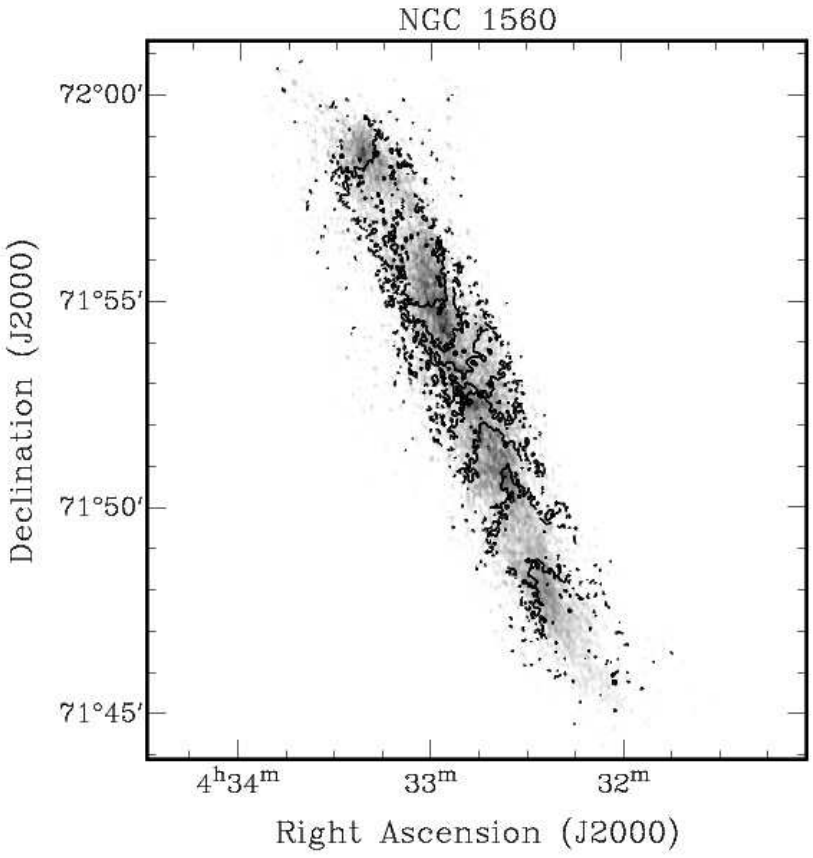

Figure 6. High-resolution total HI map (greyscale) and velocity field (contours). Contours are centred around -36 km s^{-1} and spaced by 15 km s^{-1}.

$$\mu(x) = \frac{x}{1+x} \quad (7)$$

which has been shown to yield more realistic fits than the "standard" $\mu(x)$ (Sanders & Noordermeer 2007, Famaey et al. 2007b, Angus, Famaey & Diaferio 2010), which has the following form:

$$\mu_{\rm standard}(x) = \frac{x}{\sqrt{1+x^2}} \quad (8)$$

Because the estimates of the distance of NGC 1560 span a large range of values in the literature (see Section 1), in the MOND fits we decided to leave it as a free parameter, checking *a posteriori* the validity of the best-fit value.

6 MASS MODELLING RESULTS

Figures 10-12 show the mass modelling results. The Burkert halo gives a very good fit to the rotation curve ($\chi^2_{\rm red} = 0.33$), with a core radius of 5.6 kpc and a central density of 0.8×10^{-24} g cm^{-3}. However, because of the halo dominance already at small radii, it does not manage to explain the "wiggle" around 300″: the total rotation curve that results from the mass modelling with a Burkert halo is featureless, whereas the observed rotation curve is not. Note, however, that the best-fit curve goes through the (conservative) errorbars in the region of the wiggle. The best-fit stellar $M/L_{\rm I}$ ratio is 2.3, at the high end of the allowed range (see Section 5.1).

On the other hand, modelling the rotation curve using the halo predicted in ΛCDM simulations results in a bad quality fit (Fig. 11). The best-fit virial mass is $(4.4\pm0.4)\times10^{10}$ M$_\odot$ (the concentration is derived through eq. 3), which is consistent with studies linking the stellar and dark halo masses (e.g. Shankar et al. 2006, Guo et al. 2010). As in numerous galaxy rotation curves, the observed shape of the rotation curve is very different from the one predicted using an NFW halo, in particular in the innermost parts. The best-fit stellar $M/L_{\rm I}$ ratio is 0.9, which is at the lower extreme of the range of $M/L_{\rm I}$ we considered. The quality of the NFW can improve if we take both the concentration and the virial mass as free parameters. However, the price to pay is to have a best-fit virial mass of 3.0×10^{11} M$_\odot$, which is much too high for a galaxy with a stellar mass around 5×10^8 M$_\odot$ (Shankar et al. 2006, Guo et al. 2010), and to have a best-fit concentration parameter of 6.1, which is 2 σ to 2.5 σ below the scatter in the virial mass-concentration relation (eq. 3) found in ΛCDM simulations (Bullock et al. 2001, Neto et al. 2007).

The so-called Einasto halo (Einasto 1965, Navarro et al. 2004, Navarro et al. 2009), which is a functional form that gives a slightly better description of the density distribution simulated halos than the NFW formula, was not used here. The reason is that within the radial range probed by our data ($0.02r_{\rm max}$ to $0.73r_{\rm max}$, where $r_{\rm max}$=2.16$r_{\rm s}$ and $r_{\rm s}$ is derived from the best-fit $M_{\rm vir}$ (with the concentration fixed) and eqs. 3-5), following Navarro et al. (2004, 2009) we find that the velocity difference between the two profiles is $\lesssim 0.1$dex, and it would make the velocity in the innermost parts higher, so the agreement with the data would be even *worse*.

MOND fits the rotation curve very well; we recall that we use the simple interpolating function (eq. 7). Formally, the reduced χ^2 value (0.56) is a little higher than the Burkert halo fits, but because

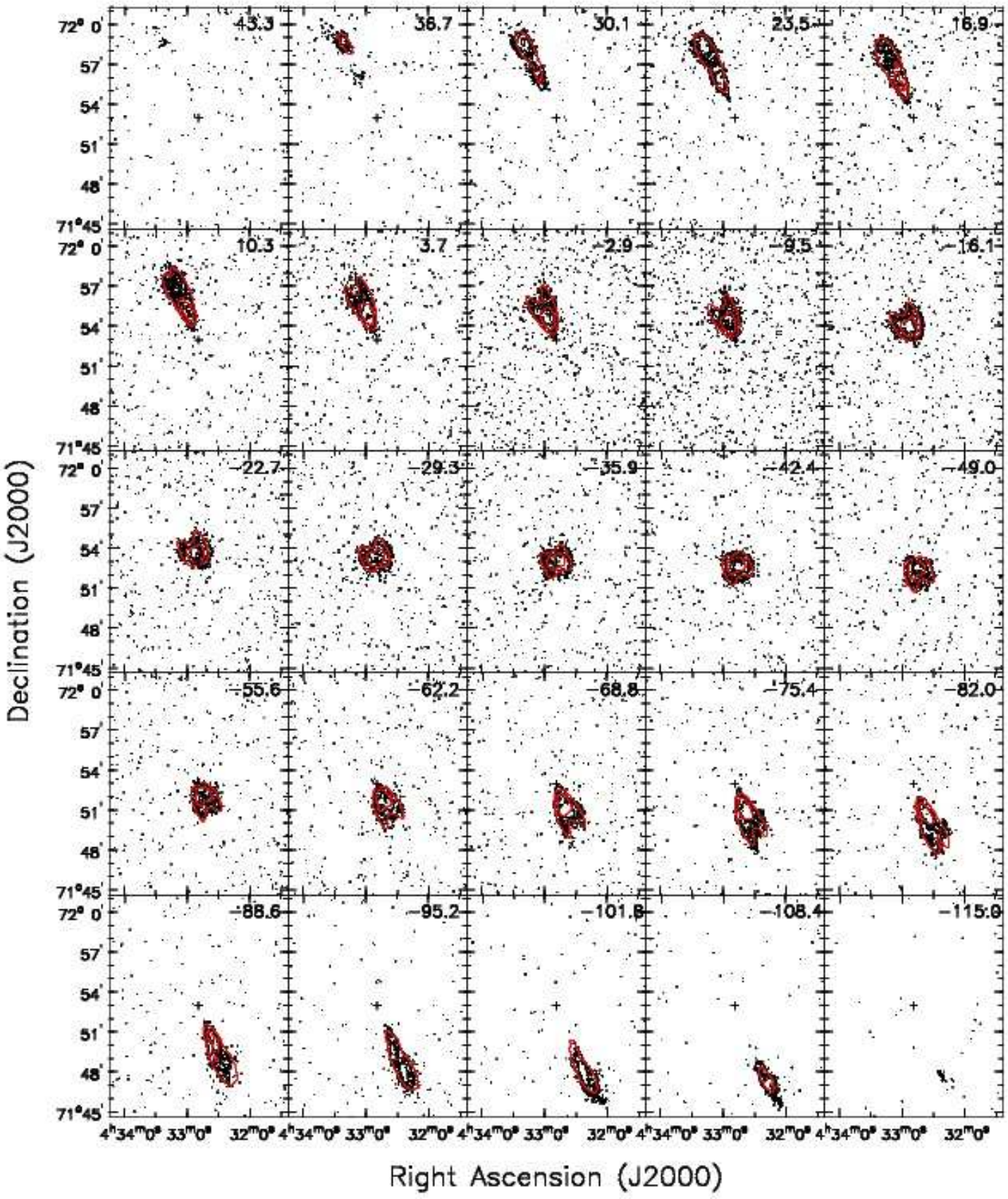

Figure 7. Same as Fig. 1, with the addition of red contours, which represent our model datacube.

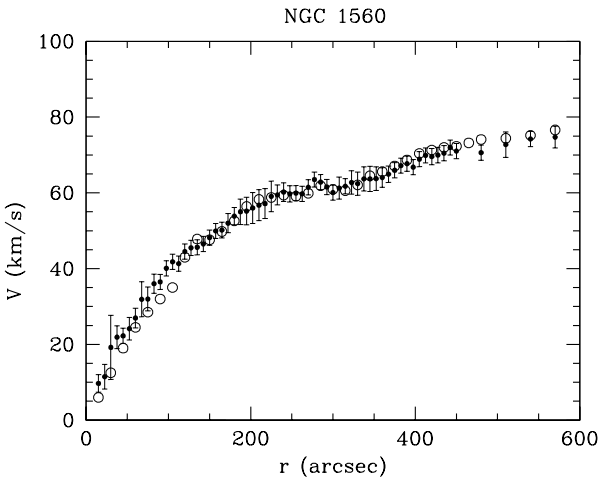

Figure 8. Comparison between the rotation curve of Broeils (1992) (empty circles) and the rotation curve derived in the present paper (full circles).

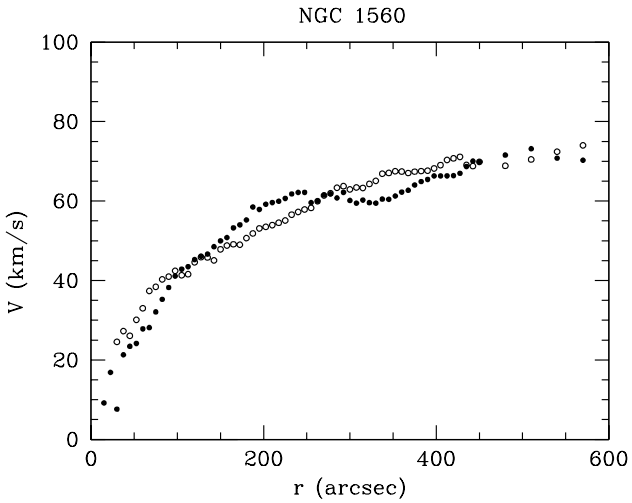

Figure 9. Rotation curve of NGC 1560 determined for the two sides separately. Empty circles represent the southern (approaching) side, whereas full circles represent the northern (receding) side.

the "wiggle" around 300″ appears both in the total rotation curve and in $V_{\rm gas}$, the MOND fit reproduces reasonably well the wiggle. The best-fit stellar $M/L_{\rm I} = 0.98$ lies within the range derived from stellar population synthesis. The best-fit distance (2.94 Mpc) is a little bit low compared with the value given in Karachentsev et al. (2003), i.e. 3.45 Mpc. However, the quality of the fit only slightly decreases (reduced χ^2=0.69) if we force the distance to stay within the range allowed by Karachentsev et al. (2003). Also, we note that there are also lower estimates of NGC 1560's distance, e.g. Lee & Madore (1993), who give 2.5 Mpc using the brightest stars method. Using the standard interpolating function (eq. 8) gives a slightly higher best-fit distance (3.16 Mpc) and stellar $M/L_{\rm I}$ ratio (1.09), for an equivalently good fit (χ^2=0.54, not shown here).

It has been noted in the past (e.g. Bosma 1999) that there are cases where wiggles are linked to non-circular motions due to spiral arms. Obviously, this effect is much more prominent in long-slit data than in two-dimensional velocity fields. Bosma mentions Visser (1980), where in M81 strong non-circular motions in a 2-D velocity field still have a (small) effect on the rotation curve. However, in the case of NGC 1560 there are non-prominent spiral arms, so we expect the effect on the rotation curve to be very small, certainly not as large as the observed wiggle.

At the radius of the wiggle, the orbital frequency is ∼14 km s^{-1} kpc^{-1} and the epicyclic frequency is ∼21 km s^{-1} kpc^{-1}, which means that the mass distribution has the time to react to the gravitational potential from one side of the galaxy to the other, but only barely. Hence, it is interesting (though not formally completely correct, the construction of a rigorous model goes beyond the scope of this paper) to make mass models of the two sides (approaching and receding) of the galaxy independently, as if the two sides were separate and in independent circular motion. We kept the distance fixed at 2.94 Mpc, the best-fit distance in the total MOND fit. The results are shown in Fig. 13, where one can notice that the observed kinematics follows the distribution of baryons, even when the two sides are considered separately: in the receding (northern) side of the galaxy, the wiggle in the baryons distribution is much more pronounced, and this is reflected in the observed kinematics of that side of the galaxy.

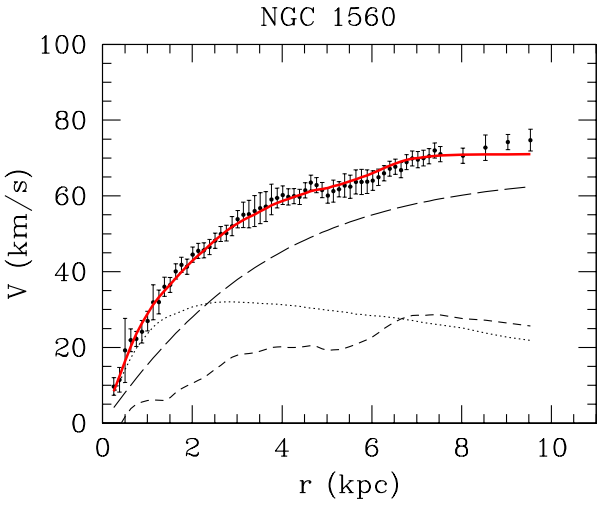

Figure 10. Rotation curve fit using the Burkert halo. Short-dashed, dotted, and long-dashed lines represent the Newtonian contributions of the gaseous disk, stellar disk, and dark halo, respectively. The best-fit model is shown as a solid red line.

7 CONCLUSIONS

NGC 1560 is a nearby dwarf Sd galaxy, whose rotation curve has a very distinct "wiggle". We observed NGC 1560 in HI with the GMRT, achieving a two times better resolution than the previous data of Broeils (1992), which were obtained with the WSRT.

We re-derived the rotation curve of NGC 1560 by taking projection effects into account (because of its high inclination angle, $\sim 80^\circ$), and checked the reliability of our findings by creating model datacubes, which were compared to the observations.

The new rotation curves is similar to the one derived by Broeils (1992), the main differences being in the innermost $\sim 100''$: at those radii we find slightly ($\lesssim 5$ km s^{-1}) higher velocities than Broeils (1992). Also, we confirm the presence of a "wiggle" in the rotation curve, at around 300″.

The rotation curve was then corrected for asymmetric drift and

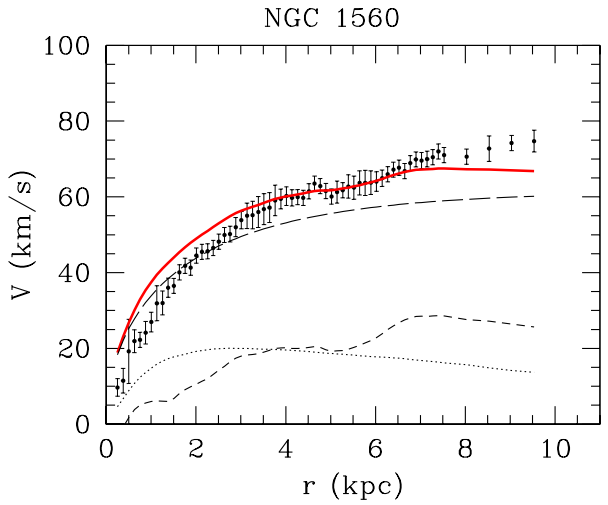

Figure 11. Rotation curve fit using the NFW halo. Lines and symbols are like those in Fig. 10.

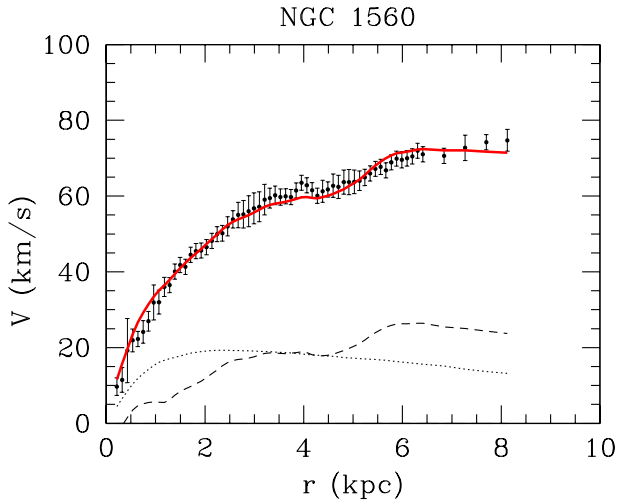

Figure 12. Rotation curve fit using MOND. The best-fit distance is 2.94 Mpc. Lines and symbols are like those in Fig. 10.

used as input for mass modelling. The contribution of the stellar disk to the rotation curve was derived from NIR (I-band) data. The core-dominated Burkert halo gives a good fit to the observed rotation curve, but it does not manage to explain the wiggle. The NFW halo gives a bad fit, greatly overpredicting the velocity in the innermost regions and slightly underpredicting the outermost ones; using an Einasto halo would only slightly change the fits, making them marginally even worse. MOND gives a very good account of the data, particularly of the wiggle.

HI observations at about twice the spatial resolution of the previous ones confirmed thus that NGC 1560 is a nice example of the connection between baryons and total kinematics in galaxies (an expression of which is MOND).

ACKNOWLEDGEMENTS

GG and KVA are postdoctoral researchers of the FWO-Vlaanderen (Belgium). BF is a Senior Research Associate of the CNRS (France). We thank the referee, Stacy McGaugh, for insightful comments that improved the quality of this paper. We thank the staff of the GMRT who have made these observations possible. GMRT is run by the National Centre for Radio Astrophysics of the Tata Institute of Fundamental Research.

REFERENCES

Angus, G. W., Shan, H. Y., Zhao, H. S., & Famaey, B. 2007, ApJ, 654, L13
Angus, G. W., Famaey, B., & Diaferio, A. 2010, MNRAS, 402, 395
Barbieri, C. V., Fraternali, F., Oosterloo, T., Bertin, G., Boomsma, R., & Sancisi, R. 2005, A&A, 439, 947
Begeman, K. G., 1989, A&A, 223, 47
Begeman, K. G., Broeils, A. H., Sanders, R. H., 1991, MNRAS, 249, 5 23
Bell, E. F., de Jong, R. S., 2001, ApJ, 550, 212
Bienaymé, O., Famaey, B., Wu, X., Zhao, H. S., & Aubert, D. 2009, A&A, 500, 801
Blumenthal, G. R., Faber, S. M., Flores, R., & Primack, J. R. 1986, ApJ, 301, 27
Bosma, A. 1999, Galaxy Dynamics - A Rutgers Symposium, 182, 339
Broeils, A. H. 1992, A&A, 256, 19
Bryan, G. L., Norman, M. L., 1998, ApJ, 495, 80
Bullock, J.S., Kolatt, T.S., Rachel, Y.S., Somerville, S., Kravtsov, A.V., Klypin, A.A., Primack, J.R., Dekel, A., 2001, MNRAS, 321, 559
Burkert, A., 1995, ApJ, 447, L25
Corbelli, E., Lorenzoni, S., Walterbos, R. A. M., Braun, R., & Thilker, D. A. 2010, A&A, in press (arXiv:0912.4133)
de Blok, W. J. G., McGaugh, S. S., Rubin, V. C., 2001, AJ, 122, 2396
de Jong, R. S., & Bell, E. F. 2007, Island Universes - Structure and Evolution of Disk Galaxies, 107
de Vaucouleurs, G., et al. 1991, Revised Catalogue of Galaxies Version 3.9 (RC3.9)
Donato, F., et al. 2009, MNRAS, 397, 1169
Einasto J., 1965, Trudy Inst. Astroz. Alma-Ata, 51, 87
Famaey, B., & Binney, J. 2005, MNRAS, 363, 603
Famaey, B., Bruneton, J.-P., & Zhao, H. 2007a, MNRAS, 377, L79
Famaey, B., Gentile, G., Bruneton, J.-P., & Zhao, H. 2007b, Phys. Rev. D, 75, 063002
Gentile, G., Salucci, P., Klein, U., Vergani, D., Kalberla, P., 2004, MNRAS, 351, 903
Gentile, G., Burkert, A., Salucci, P., Klein, U., Walter, F., 2005, ApJ, 634, L145
Gentile, G., Salucci, P., Klein, U., & Granato, G. L. 2007a, MNRAS, 375, 199
Gentile, G., Famaey, B., Combes, F., Kroupa, P., Zhao, H. S., & Tiret, O. 2007b, A&A, 472, L25
Gentile, G. 2008, ApJ, 684, 1018
Gentile, G., Famaey, B., Zhao, H., & Salucci, P. 2009, Nature, 461, 627
Gnedin, O. Y., Kravtsov, A. V., Klypin, A. A., & Nagai, D. 2004, ApJ, 616, 16

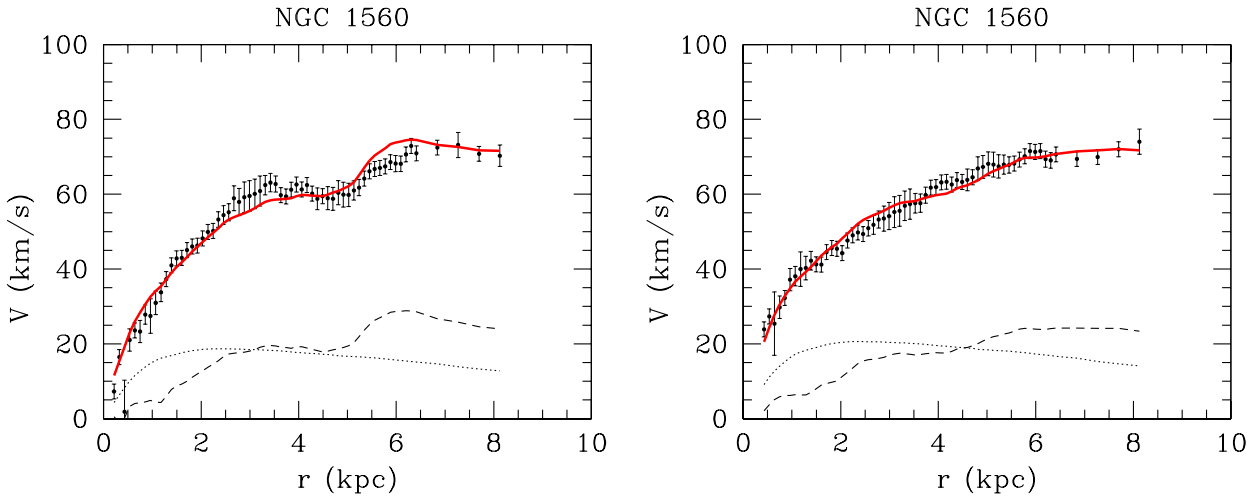

Figure 13. Rotation curve fits using MOND, fitting separately the two sides of the galaxy and using the simple interpolation function. On the left is the northern (receding) side of the galaxy, on the right is the southern (approaching) side. Lines and symbols are like those in Fig. 10.

Governato, F., et al. 2010, Nature, in press (arXiv:0911.2237)

Greisen, E. W., Spekkens, K., & van Moorsel, G. A. 2009, AJ, 137, 4718

Guo, Q., White, S., Li, C., & Boylan-Kolchin, M. 2010, MNRAS, 367

Karachentsev, I. D., Sharina, M. E., Dolphin, A. E., & Grebel, E. K. 2003, A&A, 408, 111

Kregel, M., van der Kruit, P. C., & de Grijs, R. 2002, MNRAS, 334, 646

Krismer, M., Tully, R. B., & Gioia, I. M. 1995, AJ, 110, 1584

Kuzio de Naray, R., McGaugh, S. S., de Blok, W. J. G., & Bosma, A. 2006, ApJS, 165, 461

Lee, M. G., & Madore, B. F. 1993, AJ, 106, 66

Marchesini, D., D'Onghia, E., Chincarini, G., Firmani, C., Conconi, P., Molinari, E., & Zacchei, A. 2002, ApJ, 575, 801

Mashchenko, S., Couchman, H. M. P., & Wadsley, J. 2006, Nature, 442, 539

McGaugh, S. S., & de Blok, W. J. G. 1998, ApJ, 499, 66

McGaugh, S. S., Schombert, J. M., Bothun, G. D., & de Blok, W. J. G. 2000, ApJ, 533, L99

McGaugh, S. S. 2005a, Phys. Rev. Letters, 95, 171302

McGaugh, S. S. 2005b, ApJ, 632, 859

McMillan, P. J., & Dehnen, W. 2005, MNRAS, 363, 1205

Milgrom, M., 1983, ApJ, 270, 365

Milgrom, M., & Sanders, R. H. 2003, ApJ, 599, L25

Navarro, J.F., Frenk, C.S., White, S.D.M., 1996, ApJ, 462, 563

Navarro, J. F., et al. 2004, MNRAS, 349, 1039

Navarro, J. F., et al. 2009, MNRAS, 1918

Neto, A. F., et al. 2007, MNRAS, 381, 1450

Persic, M., Salucci, P., & Stel, F. 1996, MNRAS, 281, 27

Salucci, P., & Burkert, A. 2000, ApJ, 537, L9

Salucci, P., Lapi, A., Tonini, C., Gentile, G., Yegorova, I., & Klein, U. 2007, MNRAS, 378, 41

Sancisi, R., & Allen, R. J. 1979, A&A, 74, 73

Sancisi, R. 2004, Dark Matter in Galaxies, 220, 233

Sandage, A. 1988, ApJ, 331, 605

Sanders, R. H., & Noordermeer, E. 2007, MNRAS, 379, 702

Sellwood, J. A., & McGaugh, S. S. 2005, ApJ, 634, 70

Sellwood, J. A. 2008, ApJ, 679, 379

Shankar, F., Lapi, A., Salucci, P., De Zotti, G., & Danese, L. 2006, ApJ, 643, 14

Skillman, E. D., Bothun, G. D., Murray, M. A., & Warmels, R. H. 1987, A&A, 185, 61

Tamburro, D., Rix, H.-W., Leroy, A. K., Low, M.-M. M., Walter, F., Kennicutt, R. C., Brinks, E., & de Blok, W. J. G. 2009, AJ, 137, 4424

Tiret, O., Combes, F., Angus, G. W., Famaey, B., & Zhao, H. S. 2007, A&A, 476, L1

Verheijen, M. A. W., & Sancisi, R. 2001, A&A, 370, 765

Visser, H. C. D. 1980, A&A, 88, 149

Wechsler, R. H., Bullock, J. S., Primack, J. L., Kravtsov, A. V., Dekel, A., 2002, ApJ, 568, 52

Weinberg, M. D., & Katz, N. 2002, ApJ, 580, 627

Zhao, H. S., & Famaey, B. 2006, ApJ, 638, L9